Superhigh-Resolution Recognition of Optical Vortex Modes Assisted by a Deep-Learning Method

Zhanwei Liu,[*] Shuo Yan,[*] Haigang Liu,[†] and Xianfeng Chen[‡]

State Key Laboratory of Advanced Optical Communication Systems and Networks, School of Physics and Astronomy, Shanghai Jiao Tong University, Shanghai 200240, China

Orbital angular momentum (OAM) has demonstrated great success in the optical communication field, which theoretically allows an infinite increase of the transmitted capacity. The resolution of a receiver to precisely recognize OAM modes is crucial to expand the communication capacity. Here, we propose a deep learning (DL) method to precisely recognize OAM modes with fractional topological charges. The minimum interval recognized between adjacent modes decreases to 0.01, which as far as we know is the first time this superhigh resolution has been realized. To exhibit its efficiency in the optical communication process, we transfer an Einstein portrait by a superhigh-resolution OAM multiplexing system. As the convolutional neuron networks can be trained by data up to an infinitely large volume in theory, this work exhibits a huge potential of generalized suitability for next generation DL based ultrafine OAM optical communication, which might even be applied to microwave, millimeter wave, and terahertz OAM communication systems.

Vortex beams carrying orbital angular momentum (OAM) have been extensively investigated in optical manipulation [1], imaging [2], interaction between light and matter [3,4], and optical communication [5] since it was recognized in 1992 [6]. The helical wave front of such a vortex beam is described by a phase factor $\exp(i\ell\phi)$, where ϕ is the azimuthal angle and the topological charge ℓ is an unlimited integer or fractional value. Owing to the unbounded dimensional space, it provides high degrees of freedom for multiplexing information, which infinitely boosts the transmitted capacity in optical communication processes [7,8].

Because of its significant application, the generation of OAM states has aroused tremendous enthusiasm ranging from spiral phase plate [9], q plate [10,11], and metasurface [12] to integrated devices [13]. One of the most accomplished types of technology is to use spatial light modulator (SLM) uploading spiral holograms [14], which can simply create vortex beams and flexibly manipulate the phase information of light. Besides, the recognizable ability of the receiver is also crucial for both OAM shift keying (OAM-SK) [15] and OAM division multiplexing (OAM-DM) [16] in terms of OAM-based optical communication. Therefore, much work has been conducted focusing on efficiently developing an OAM sorter recently. Some techniques utilize traditional optics theories that transform the azimuthal position into transverse position [17] based on interferometers [18–20] and vortex diffractive gratings [21]. One currently efficient sorting method is to implement coordinate transformation that separates states with different topological charges by a distinct focal spot on the detect

plane [22,23]. And a computational method to measure the transmission matrix (TM) provides an anti-interference approach to retrieve the propagation of vortex beams [24]. In addition, the OAM-to-polarization coupling effect is also proposed to sort different OAM states of light [25]. All those methods pave the way for effective OAM-based optical communication.

However, owing to the limitation of the resolution, only eigenmodes where topological charges are integers are considered in all methods mentioned above. With the increase of an integer topological charge value, the growing phase singularity and the diffraction effect enormously affects the intensity distributions of vortex beams, which extremely adds the difficulties of being focused in free-space and being coupled in fibers. This problem limits the development of the OAM-based optical communication. Consequently, it is of fundamental importance to expand communication capacity adequately with more OAM states but smaller phase singularity.

Our goal here is to develop a superhigh-resolution technique to precisely separate modes into subdivisible space between adjacent eigenmodes. That is, the minimum interval $\Delta\ell$ among recognized modes is a fractional value and can be as small as possible. The pioneering techniques of generating fractional OAM modes were proposed in 2004 [26,27]. However, the tiny variety of fractional OAM modes is further complicated to be discriminated compared to that of integer changes [28–30]. Recently, the deep learning (DL) method has been developed to possess the ability of extracting intrinsic features and dividing decision boundary according to data [31]. The original assignment

for DL is to optimize a classification problem that is consistent with our task, which has gained great achievements [32–34]. Moreover, this end-to-end framework efficiently simplifies the optical system with simultaneous low-power loss. In recent literature, the combination of DL and optics has been rapidly growing [35]. Reconstructing images through scattering media [36–38] with highly scalable DL approaches have been demonstrated in experiments to exhibit steady transmission processes in optical configuration.

In this Letter, we perform an OAM-recognition neuron network (ORNN) with DL to enormously improve the OAM recognizable resolution. The ORNN is first designed to exactly extract features of different fractional vortex beams and then acquire the decision boundary for discrimination. To evaluate its generalized performance, we then simulate an optical parallel communication system to transmit data by encoded OAM superstates in which each mode is regarded as one bit. Because of the slight difference among encoded bits and the high recognizable accuracy, one superstate can theoretically carry infinite amounts of data. The experimental $<0.02\%$ bit error ratio (BER) verifies the feasibility of expanding communication capacity in this approach.

The phase recognition assignment can be simply comprehended because of the end-to-end characteristic. According to Fraunhofer diffraction, the complex field $U(x, y)$ carrying phase information from the diffractive object to the imaging plane can be described by

$$U_{\text{out}}(x,y) = \frac{\exp(ikz)}{i\lambda z}\exp\left(\frac{ik}{2z}(x^2+y^2)\right)$$
$$\times \iint U_{\text{in}}(x_0, y_0)\exp\left(-\frac{i2\pi}{\lambda z}(xx_0+yy_0)\right)dx_0dy_0$$
$$= \hat{H}U_{\text{in}}(x_0, y_0), \qquad (1)$$

where k is the wave number, z is the distance between the object and imaging plane, λ is the wavelength, and $\hat{H}$ is the forward operator of the above optical process. After the propagation described by Eq. (1), the measured intensity of the vortex mode is derived as

$$I_{\text{out}} = |U_{\text{out}}|^2 = |\hat{H}U_{\text{in}}|^2. \qquad (2)$$

I_{out} can be recorded by camera as the form of an intensity matrix in which each element is related to the phase information of U_{in}. Then I_{out} is inputted into ORNN to predict an estimate of the topological charge value $p = \hat{F}I_{\text{out}}$, where the operator $\hat{F}$ represents the calculation process of ORNN. The prediction is obtained by successive extracting the features of I_{out}. And the optimization target is to iteratively minimize the objective function that can be described by the form of
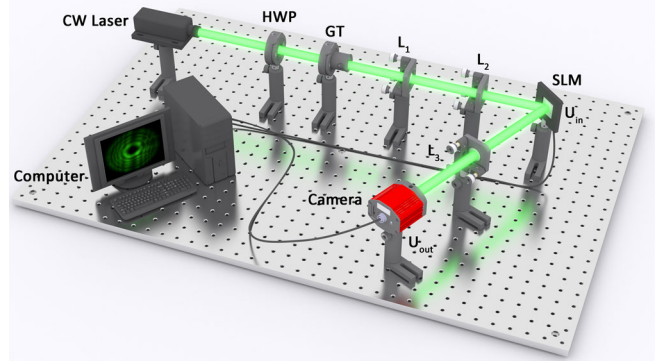
FIG. 1. Experimental setup (see the text for more details).

$$\min_{\theta} J(\ell, p) + \alpha\hat{F}(\theta). \qquad (3)$$

Here, $J(\ell, p)$ is designed to compare the true topological charge value ℓ with the prediction p, and θ is the collection of all weight parameters in ORNN (see in Supplemental Material Note 1 [39]). θ will be updated to make p equal to ℓ when the training process is convergent. The second term containing α is to regularize what was acknowledged prior by restraining the influence from θ on the optimization.

The experimental setup is shown in Fig. 1. The linear polarized light is delivered from a continuous wave (cw) laser source (532 nm wavelength; 1.2 mm waist; <1.5 mrad divergence) with power of 4.7 mW. A half-wave plate (HWP) and a Glan-Taylor (GT) prism are used to control the polarization and the intensity of light. Then lens L_1 (30 mm) and L_2 (200 mm) form a telescope for expanding the light to illuminate the SLM. The SLM in our experiment has a resolution of 1920×1080 pixels, each with a square area of 8×8 μm^2. Phase holograms are uploaded on SLM to generate fractional OAM states. After being reflected by SLM, the wave front has been transformed to $U_{\text{in}} \sim \exp(i\ell\phi)$; here ℓ is a fractional value. Limited by the resolution of our SLM, $\Delta\ell = 0.01$ almost reaches the smallest variation that can be displayed between adjacent OAM states. So it is regarded as the minimum separation to be recognized in our optimization problem. The modulated light is propagated through L_3 (50 mm) and then is recorded by a CMOS camera which has 2448×2048 pixels with size of 3.45×3.45 μm^2. The recorded intensity distributions I_{out} cover the phase information of the fractional vortex beams (U_{in}) according to Eqs. (1) and (2). Finally, I_{out} is down sampled to 224×224 pixels to be inputted into ORNN.

The architecture of ORNN is shown in Fig. 2. Its details are provided in the Supplemental Material, Note 2 [39]. Our classification task requires the highly precise recognition of a fractional topological charge interval between adjacent OAM modes. Nevertheless, the difference of I_{out} is too small to be distinguished. The used average pooling layer [34] causes the tiny difference to be even less obvious.
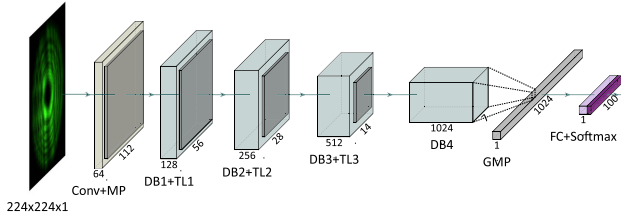
FIG. 2. Sketch map of the ORNN architecture to recognize OAM modes. The boxes indicate the number and size of extracted feature maps from hidden layers, which are not tangible objects. A 7×7 convolution layer with 2 strides (Conv); max pooling layer with 2 strides (MP); dense block (DB); transition layer, containing a max pooling layer behind 1×1 convolution (TL); Global max pooling layer (GMP); fully connected layer (FC).

Therefore, we select the max pooling layer [32] for down sampling to magnify the weak variance when topological charge changes. The objective function to be optimized in Eq. (3) is defined by

$$J(\ell, p) = -\frac{1}{m}\left[\sum_{i=1}^{m}\sum_{j=1}^{n} 1\{\ell^{(i)} = k_j\} \log\left(\frac{\exp(p_j)}{\sum_{t=1}^{n} \exp(p_t)}\right)\right],$$

(4)

where m is the total number of the recorded dataset, $\ell^{(i)}$ is the label of the ith intensity distribution I_{out}, and the set $\{k_0, k_1, \ldots, k_n\}$ represents the topological charge value used in our experiments. The expression $1\{\ell^{(i)} = k_j\}$ means it will take value 1 when condition $\{\ell^{(i)} = k_j\}$ is satisfied and 0 for the opposite case.

For adequately exploiting the bandwidth resources of the OAM modes, we first perform the ORNN to distinguish OAM modes with fractional intervals of topological charge. To prepare adequate data for training, one OAM mode is augmented with different initial phases, which can mean-while improve the rotary robustness of ORNN. The initial phase of each mode in this experiment is changed from 0 to 1.98π with $\Delta\phi = 0.02\pi$. Besides, considering the computational capability and the visualized presentation, we select the OAM modes from $\ell = 1.00$ to $\ell = 1.99$ with $\Delta\ell = 0.01$ as the state interval to be discriminated. Totally, the full dataset contains 10 000 OAM modes labeled by 100 different topological charges. In addition, 10% of each value is randomly sampled in the test dataset that never participates in the training process. The weight parameters θ in ORNN are trained using a stochastic gradient descent (SGD) optimizer with batch size 16 for 100 epochs. The initial learning rate is set to be 0.001, and is lowered by 10 times at epoch 80 and epoch 90. A $\mathcal{L}2$ regularization is placed in the fully connected layer with weight decay of 0.01 to prevent overfitting as the role of α in Eq. (3) [36].

After training, the test OAM modes are inputted into ORNN for evaluating the classification performance. Figure 3(a) shows four pairs of the gray scale phase
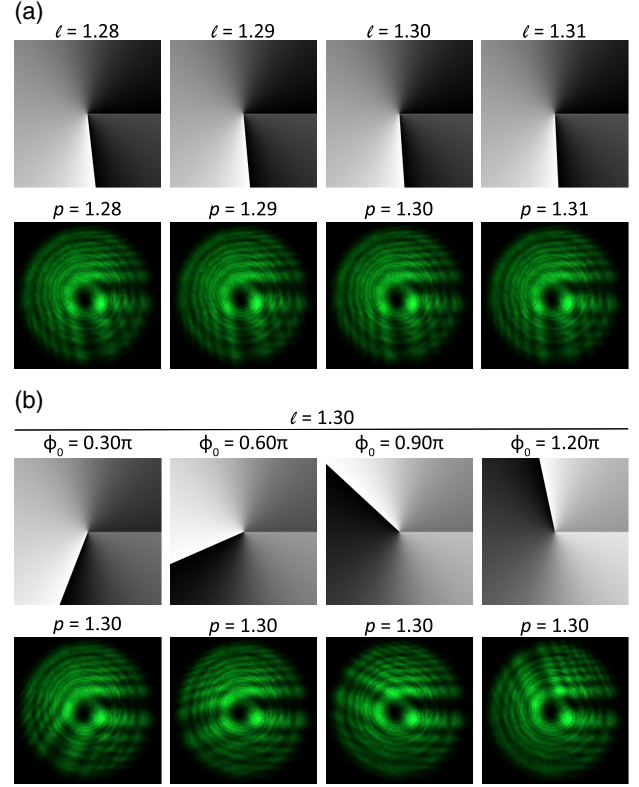
FIG. 3. The recognized OAM modes with fractional topological charge. (a) Adjacent modes with 0.01 steps that can be distinguished exactly. First row: Phase pictures uploaded on the SLM. Second row: The intensity distributions of vortex modes recorded by the CMOS camera. (b) Arranged same as (a), except it shows the same OAM modes with different initial phase.

hologram and the corresponding intensity distributions of the OAM mode with 0.01 state interval. The annotation demonstrates good agreement between actual topological charges and predictions, indicating that the invisible difference between adjacent modes is seized easily by the trained ORNN. This is because the convolution operation and the max pooling operation continuously extract and magnify the tiny variation in the 224×224 matrix, even though the most part on I_{out} of the fractional vortex beams looks similar. In Fig. 3(b), the same OAM mode with a different initial phase results in the same prediction from ORNN, which shows the ability of extracting the general feature of the vortex beams. To show an example of the detailed classification performance, a confused matrix [35] from $\ell = 1.25$ to $\ell = 1.34$ is reported, as shown in Fig. 4(a). Almost all tested OAM modes are recognized correctly with only one wrong prediction lying in the adjacent OAM state, demonstrating that the small separation in this experiment can also be segmented clearly. Another quantitative analysis of ORNN is shown in Fig. 4(b). 98% accuracy is finally achieved by using the max pooling layer to down sampling. The improvement at epoch 80 is attributed to the lowered learning rate. In addition, the
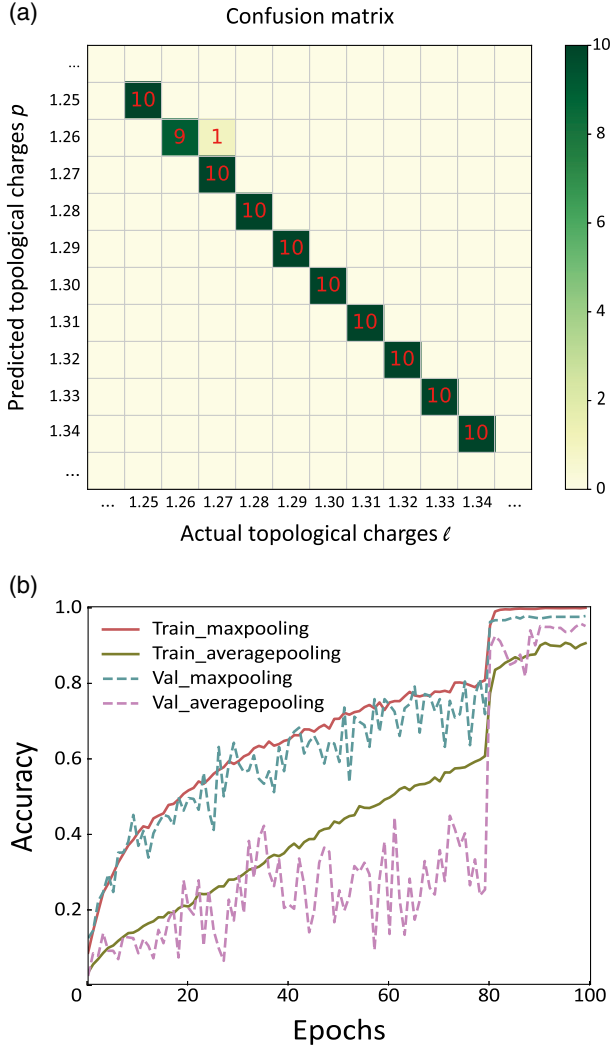
FIG. 4. Quantitative analysis of ORNN. (a) Confusion matrix from $\ell = 1.25$ to $\ell = 1.34$. (b) The accuracy curves of using the max pooling layer and average pooling layer.

FIG. 5. (a) An 8-bit OAM superstate multiplexed demonstration encoded by fractional modes. (b) Detailed process of transmitting an Einstein portrait utilizing the superhigh-resolution OAM multiplexing system.

accuracy curve using the average pooling layer is also presented for comparison. The wide fluctuation and low accuracy in this configuration behave worse for extracting the characteristics in this task. This classification performance can be further improved by deepening DNN architecture or expanding the dataset to become more numerous and more diversified. Notably, the unique OAM modes in the whole dataset mean that every test mode has not been seen by ORNN before, but it still recognizes the unseen initial phase at a high performance which confirms the rotary robustness for different OAM modes.

To further demonstrate the availability of our method in exploiting fractional OAM modes, we experimentally implement a superhigh-resolution OAM multiplexing system. Same as the experimental setup discussed above, the system simulates a 2 m free-space communication environment, which is based on fractional OAM superstates

with adjacent interval $\Delta\ell = 0.01$. We encode an 8-bit binary byte using 8 different OAM modes, the topological charge of which is chosen from $\ell = 1.93$ to $\ell = 2.00$. Each bit value is assigned to be 1 or 0 on the basis of whether the corresponding mode exists or not. Specifically, the multiplexed superstate is generated by $\ell_{\text{mul}} = \sum_{i}^{8} (\ell_i/N)$, where N is the number of "1" in this 8-bit data as shown in Fig. 5(a). We record the $2^8 = 256$ multiplexed superstates for 50 loops and, in total, $256 \times 50 = 12\,800$ data are fabricated. After training, perfectly quantified 100% test accuracy is achieved without any manual intervention. As Fig. 5(a) shows, an 8-bit code only occupies a small region on I_{out} of the superstate, which indicates that large capacity can continuously be used to encode. Moreover, the vortex beam still remains at normal intensity distributions even if we are multiplexing more modes in our method. Then, we transfer an image using above a completed free-space system to further verify its performance. A gray scale image of an Einstein portrait with 110×100 pixels shown in the left of Fig. 5(b) is chosen in our experiment. Each pixel value is related to a 0–255 integer represented by an 8-bit superstate to be transmitted through the superhigh-resolution OAM multiplexing system. The 11 000 sequential codes are sent to ORNN to predict every pixel value with <0.02% BER as Fig. 5(b) shows.

Especially in considering fiber propagation, various forms of environmental disturbance drastically aggravate the distortion of signal. In fact, the instability of our laser

source and optical system results in that the same OAM mode sampled at different times has different I_{out}, which simulates the mentioned distortion to some extent. For solving this problem, we extend the time interval while recording data to cover the disturbance. The high performance in Fig. 5(b) shows the ORNN can extract the intrinsic features with neglecting disturbances in our system, which expresses tremendous possibilities for covering the influence of propagating in fiber. Moreover, the turbulent atmosphere in free space transition of long distance can also be implemented, combining with the common used phase compensation method of adaptive optics.

The method proposed here shows its powerful ability to distinguish ultrafine OAM modes that traditional approaches cannot realize. Indeed, the low frame rate of the camera (35 fps at full resolution) and SLM (75 Hz) are the main limitations for the rate of transference comparing to accomplished OAM-DM technology [7,8,16]. However, the capacity of communication in our encoded method can be further increased by combining wavelength-division multiplexing (WDM) and polarization multiplexing (PM). And the transmitting rate can also be further improved by the higher frame rate of the device. In addition, due to the high performance of recognizing fractional modes, the ORNN possesses the enormous potential for multiplexing as many modes with 0.01 intervals as possible, which unlimitedly expands the communication capacity in theory. More importantly, challenges that existed in previous integer-topological-charge OAM-based optical communication, such as beam divergence, aperture size, and misalignment of transmitter and receiver, can be solved by using the fractional topological charge ORNN proposed here.

In conclusion, we realize superhigh-resolution recognition of OAM by ORNN. Such an end-to-end method has been demonstrated to be robust and generalized for a complicated classification task. In our experiment, different OAM modes with 0.01 intervals can be precisely distinguished, and the same topological charge mode with a different initial phase can also be recognized by its corresponding topological charge. Then, we apply the ORNN to develop an expansive multiplexing technique, and evaluate it using 8-bit fractional superstates. The $<0.02\%$ BER shows this intelligent recognition concept offers new opportunities for next generation DL-based ultrafine OAM optical communication. In principle, such a method as proposed here might even be applied to microwave, millimeter wave, and terahertz OAM communication fields.

[*]These authors contributed equally to this work.
[†]liuhaigang@sjtu.edu.cn
[‡]xfchen@sjtu.edu.cn

[1] L. Paterson, M. P. MacDonald, J. Arlt, W. Sibbett, P. E. Bryant, and K. Dholakia, Controlled rotation of optically trapped microscopic particles, Science **292,** 912 (2001).

[2] B. Jack, J. Leach, J. Romero, S. Franke-Arnold, M. Ritsch-Marte, S. M. Barnett, and M. J. Padgett, Holographic Ghost Imaging and the Violation of a Bell Inequality, Phys. Rev. Lett. **103,** 083602 (2009).

[3] L. Marrucci, C. Manzo, and D. Paparo, Optical Spin-to-Orbital Angular Momentum Conversion in Inhomogeneous Anisotropic Media, Phys. Rev. Lett. **96,** 163905 (2006).

[4] K. Toyoda, F. Takahashi, S. Takizawa, Y. Tokizane, K. Miyamoto, R. Morita, and T. Omatsu, Transfer of Light Helicity to Nanostructures, Phys. Rev. Lett. **110,** 143603 (2013).

[5] C. Paterson, Atmospheric Turbulence and Orbital Angular Momentum of Single Photons for Optical Communication, Phys. Rev. Lett. **94,** 153901 (2005).

[6] L. Allen, M. W. Beijersbergen, R. J. C. Spreeuw, and J. P. Woerdman, Orbital angular momentum of light and the transformation of Laguerre-Gaussian laser modes, Phys. Rev. A **45,** 8185 (1992).

[7] J. Wang, J. Y. Yang, I. M. Fazal, N. Ahmed, Y. Yan, H. Huang, Y. Ren, Y. Yue, S. Dolinar, M. Tur, and A. E. Willner, Terabit free-space data transmission employing orbital angular momentum multiplexing, Nat. Photonics **6,** 488 (2012).

[8] N. Bozinovic, Y. Yue, Y. Ren, M. Tur, P. Kristensen, H. Huang, A. E. Willner, and S. Ramachandran, Terabit-scale orbital angular momentum mode division multiplexing in fibers, Science **340,** 1545 (2013).

[9] S. S. R. Oemrawsingh, X. Ma, D. Voigtand, A. Aiello, E. R. Eliel, G. W. Hooft, and J. P. Woerdman, Experimental Demonstration of Fractional Orbital Angular Momentum Entanglement of Two Photons, Phys. Rev. Lett. **95,** 240501 (2005).

[10] E. Nagali, F. Sciarrino, F. De Martini, L. Marrucci, B. Piccirillo, E. Karimi, and E. Santamato, Quantum Information Transfer from Spin to Orbital Angular Momentum of Photons, Phys. Rev. Lett. **103,** 013601 (2009).

[11] E. Nagali, L. Sansoni, F. Sciarrino, L. Marrucci, F. D. Martini, B. Piccirillo, E. Karimi, and E. Santamato, Optimal quantum cloning of orbital angular momentum photon qubits through Hong–Ou–Mandel coalescence, Nat. Photonics **3,** 720 (2009).

[12] E. Karimi, S. A. Schulz, I. D. Leon, H. Qassim, J. Upham, and R. W. Boyd, Generating optical orbital angular momentum at visible wavelengths using a plasmonic metasurface, Light Sci. Appl. **3,** e167 (2014).

[13] X. Cai, J. Wang, M. J. Strain, B. Johnson-Morris, J. Zhu, M. Sorel, J. L. O'Brien, M. G. Thompson, and S. Yu, Integrated compact optical vortex beam emitters, Science **338,** 363 (2012).

[14] L. Chen, J. Lei, and J. Romero, Quantum digital spiral imaging, Light Sci. Appl. **3,** e153 (2014).

[15] P. Jia, Y. Yang, C. J. Min, H. Fang, and X. C. Yuan, Sidelobe-modulated optical vortices for free-space communication, Opt. Lett. **38,** 588 (2013).

[16] H. Huang, G. Xie, Y. Yan, N. Ahmed, Y. Ren, Y. Yue, D. Rogawski, M. J. Willner, B. I. Erkmen, K. M. Birnbaum, S. J. Dolinar, M. P. J. Lavery, M. J. Padgett, M. Tur, and A. E. Willner, 100 Tbit/s free-space data link enabled by three-dimensional multiplexing of orbital angular momentum, polarization, and wavelength, Opt. Lett. **39,** 197 (2014).

[17] A. M. Yao and M. J. Padgett, Orbital angular momentum: origins, behavior and applications, Adv. Opt. Photonics **3,** 161 (2011).

[18] J. Leach, M. J. Padgett, S. M. Barnett, S. Franke-Arnold, and J. Courtial, Measuring the Orbital Angular Momentum of a Single Photon, Phys. Rev. Lett. **88,** 257901 (2002).

[19] J. Leach, J. Courtial, K. Skeldon, S. M. Barnett, S. Franke-Arnold, and M. J. Padgett, Interferometric Methods to Measure Orbital and Spin, or the Total Angular Momentum of a Single Photon, Phys. Rev. Lett. **92,** 013601 (2004).

[20] X. Gu, M. Krenn, M. Erhard, and A. Zeilinger, Gouy Phase Radial Mode Sorter for Light: Concepts and Experiments, Phys. Rev. Lett. **120,** 103601 (2018).

[21] T. Lei, M. Zhang, Y. Li, P. Jia, G. N. Liu, X. Xu, Z. Li, C. Min, J. Lin, C. Yu, H. Niu, and X. Yuan, Massive individual orbital angular momentum channels for multiplexing enabled by Dammann gratings, Massive individual orbital angular momentum channels for multiplexing enabled by Dammann gratings, Light Sci. Appl. **4,** e257 (2015).

[22] G. C. G. Berkhout, M. P. J. Lavery, J. Courtial, M. W. Beijersbergen, and M. J. Padgett, Efficient Sorting of Orbital Angular Momentum States of Light, Phys. Rev. Lett. **105,** 153601 (2010).

[23] Y. Wen, I. Chremmos, Y. Chen, J. Zhu, Y. Zhang, and S. Yu, Spiral Transformation for High-Resolution and Efficient Sorting of Optical Vortex Modes, Phys. Rev. Lett. **120,** 193904 (2018).

[24] L. Gong, Q. Zhao, H. Zhang, X. Hu, K. Huang, J. Yang, and Y. Li, Optical orbital-angular-momentum-multiplexed data transmission under high scattering, Light Sci. Appl. **8,** 27 (2019).

[25] W. Zhang, Q. Qi, J. Zhou, and L. Chen, Mimicking Faraday Rotation to Sort the Orbital Angular Momentum of Light, Phys. Rev. Lett. **112,** 153601 (2014).

[26] J. Leach, E. Yao, and M. J. Padgett, Observation of the vortex structure of a non-integer vortex beam, New J. Phys. **6,** 71 (2004).

[27] S. Tao, W. M. Lee, and X. Yuan, Experimental study of holographic generation of fractional Bessel beams, Appl. Opt. **43,** 122 (2004).

[28] N. Zhang, J. A. Davis, I. Moreno, J. Lin, K.-J. Moh, D. M. Cottrell, and X. Yuan, Analysis of fractional vortex beams using a vortex grating spectrum analyzer, Appl. Opt. **49,** 2456 (2010).

[29] D. Deng, M. Lin, Y. Li, and H. Zhao, Precision Measurement of Fractional Orbital Angular Momentum, Phys. Rev. Applied **12,** 014048 (2019).

[30] J. Zhou, W. Zhang, and L. Chen, Experimental detection of high-order or fractional orbital angular momentum of light based on a robust mode converter, Appl. Phys. Lett. **108,** 111108 (2016).

[31] Y. LeCun, Y. Bengio, and G. Hinton, Deep learning, Nature (London) **521,** 436 (2015).

[32] A. Krizhevsky, I. Sutskever, and G. E. Hinton, ImageNet classification with deep convolutional neural networks, in *Proceedings of the 25th International Conference on Neural Information Processing Systems* (Neural Information Processing Systems (NIPS), 2012), Vol. 1, p. 1097.

[33] K. He, X. Zhang, S. Ren, and J. Sun, Deep residual learning for image recognition, in *2016 IEEE Conference on Computer Vision And Pattern Recognition (CVPR)* (IEEE, New York, 2016), p. 770.

[34] G. Huang, Z. Liu, L. Maaten, and K. Q. Weinberger, Densely connected convolutional networks, in *2017 IEEE Conference on Computer Vision and Pattern Recognition (CVPR)* (IEEE, New York, 2017), p. 2261.

[35] X. Lin, Y. Rivenson, N. T. Yardimei, M. Veli, Y. Luo, M. Jarrahi, and A. Ozcan, All-optical machine learning using diffractive deep neural networks, Science **361,** 1004 (2018).

[36] S. Li, M. Deng, J. Lee, A. Sinha, and G. Barbastathis, Imaging through glass diffusers using densely connected convolutional networks, Optica **5,** 803 (2018).

[37] Y. Li, Y. Xue, and L. Tian, Deep speckle correlation: a deep learning approach toward scalable imaging through scattering media, Optica **5,** 1181 (2018).

[38] A. Goy, K. Arthur, S. Li, and G. Barbastathis, Low Photon Count Phase Retrieval Using Deep Learning, Phys. Rev. Lett. **121,** 243902 (2018).

[39] See Supplemental Material at http://link.aps.org/supplemental/10.1103/PhysRevLett.123.183902 for the method of the neuron network and the details about the architecture of ORNN, which includes Ref. [40].

[40] Y. LeCun, L. Bottou, Y. Bengio, and P. Haffner, Gradient-based learning applied to document recognition, Proc. IEEE **86,** 2278 (1998).